IET Circuits, Devices & Systems

Research Article

IET Journals
The Institution of Engineering and Technology

Widely tunable low-pass $g_m - C$ filter for biomedical applications

ISSN 1751-858X
Received on 1st March 2018
Revised 11th September 2018
Accepted on 5th October 2018
E-First on 18th February 2019
doi: 10.1049/iet-cds.2018.5002
www.ietdl.org

Jayaram Reddy Machha Krishna[1] ✉, *Tonse Laxminidhi*[1]

[1]*Department of Electronics and Communication Engineering, NITK Surathkal, Karnataka, India*

✉ *E-mail: jayaram.041@gmail.com*

Abstract: This study presents a fourth-order, low-pass Butterworth transconductor–capacitor $(g_m - C)$ filter with tunable bandwidth for biomedical signal processing front-ends. An architecture has been proposed for realising very low transconductance values with tunability. This transconductor architecture makes it possible to realise a fully differential filter without the need for explicit common-mode feedback circuit. The filter has two tuning schemes, a resistor-based tuning (*R*-tuning) and a switched transconductor-based tuning (*D*-tuning). With *R*-tuning, the bandwidth is adjustable between 1 and 70 Hz and with *D*-tuning, the tuning range is 30 mHz–100 Hz. The filter has been designed in united microelectronics corporation (UMC) 0.18 µm complementary metal–oxide–semiconductor process. In terms of figure-of-merit, the proposed filter is found to be on par with the filters reported in the literature.

1 Introduction

High-performance low-frequency filters are widely used in biomedical systems for extracting low-frequency biopotential signals while rejecting unwanted signals. Since biopotential signals are weak analogue signals with an amplitude ranging from 1 µV to 10 mV and frequency ranging from 10 mHz to 10 kHz [1], higher-order low-pass filters with low-cut-off frequencies are required to extract these signals with high quality.

The design of low-pass filters with low-cut-off frequencies are quite challenging. In integrated circuits, passive resistor-inductor-capacitor (RLC) and active-resistor-capacitor (RC) filter topologies are not preferred for low-cut-off frequencies due to the requirement of large-sized components. Switched-capacitor filters [2] are barely used as they suffer from clock feedthrough and leakage problems in advanced processes. In biomedical systems, $g_m - C$ filters are widely used to achieve low-cut-off frequencies [3, 4]. The cut-off frequency in $g_m - C$ filters is decided by the ratio g_m/C, where g_m is the transconductance of the operational transconductor amplifier (OTA) and C is the integrating capacitor. Lower-cut-off frequencies can be practically achieved by increasing C and/or decreasing g_m. The on-chip capacitance is limited to a few tens of pico-farads because of silicon area limitations. Miller effect has been utilised to increase the effective capacitance on a chip [3] but with increased complexity and power. g_m reduction techniques are commonly used to reduce the cut-off frequency. In the literature, several design techniques are proposed for OTAs to achieve low values of g_m, viz-a-viz, current division, source degeneration, multiple inputs floating gate and bulk driven [4]. These techniques have their own limitations. A detailed discussion on this has been outlined in [5].

Another technique used to reduce g_m is current cancellation [6]. Its limitations are high sensitivity to mismatch and possibility of gain inversion with the presence of a mismatch. In this paper, a novel technique to reduce g_m has been proposed to achieve low-cut-off frequencies up to a few tens of hertz. This technique along with switching can be used to realise filters with wide tunable range (few tens of millihertz to few tens of hertz, three decades at least).

The rest of this paper is organised as follows. Section 2 introduces the proposed concept of g_m a reduction method for realising the transconductor. Section 3, discusses filter realisation using the proposed OTA. Simulation results follow in Section 4. Section 5 summarises this work.

2 Proposed g_m reduction method

The structure of the OTA consists of a cross-coupled differential pair, with transistors M_1, M_2, M_3 and M_4 as an input stage. The schematic representation is shown in Fig. 1.

M_1, M_4 and M_2, M_3 form two source-coupled differential pairs. All the transistors are sized equal and are operated in sub-threshold. The two differential pairs have tail currents I_{ss1} and I_{ss2} and $I_{ss1} \simeq I_{ss2}$ such that $I_{ss1} - I_{ss2} = \Delta i$. The cross-coupled arrangement of the two differential pairs effectively offers a low transconductance and is explained as follows.

Let g_{m1}, g_{m2} be the transconductances of $M_{1,4}$ and $M_{2,3}$, respectively. Then, $g_{m1} = (I_{ss1}/2\eta V_T)$ and $g_{m2} = (I_{ss2}/2\eta V_T)$ since they are operated in the sub-threshold region [7]. The small-signal output currents i_1 and i_2 can be written as in the equations below:

$$i_1 = 0.5g_{m1}(v_{ip1} - v_{im2}) + 0.5g_{m2}(v_{im1} - v_{ip2}) \tag{1}$$

$$i_2 = -i_1 \tag{2}$$

If $v_{ip1} = v_{ip2} = v_{ip}$ and $v_{im1} = v_{im2} = v_{im}$, for differential operation with $v_{ip} = -v_{im}$, (1) can be rewritten as

$$i_1 = (g_{m1} - g_{m2})v_{ip} \tag{3}$$

Defining $g_{m,\,\mathrm{eff}} = g_{m1} - g_{m2}$ as effective low-output transconductance, one can write

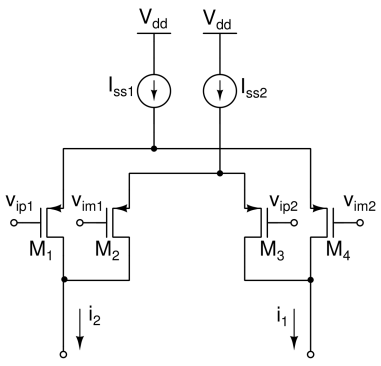

Fig. 1 *Cross-coupled differential pair*

$$g_{m,\,\mathrm{eff}} = \frac{I_{\mathrm{ss1}}}{2\eta V_{\mathrm{T}}} - \frac{I_{\mathrm{ss2}}}{2\eta V_{\mathrm{T}}} = \frac{\Delta i}{2\eta V_{\mathrm{T}}} \tag{4}$$

It is evident from (4) that $g_{m,\,\mathrm{eff}}$ is a function of Δi. Therefore, the transconductance can be made small and tuned to the bandwidth requirement of the filter. A scheme to generate tail currents I_{ss1} and I_{ss2} with a tunable difference of Δi is proposed and presented.

2.1 Tail current generation

To achieve low transconductance, the two currents I_{ss1} and I_{ss2} are to be generated in such a way that they have a very small difference Δi. The scheme proposed to achieve this is shown in Fig. 2. The circuit consists of a simple source-coupled differential pair ($M_{x1} - M_{x2}$) with inputs V_x and V_y. Drain currents of M_{x1} and M_{x2} are mirrored as tail currents I_{ss1} and I_{ss2}, respectively, with a mirroring ratio 'k'. Then, the Δi can be defined as

$$\Delta i = k g_{m,\,x}\left(V_x - V_y\right) \tag{5}$$

where $g_{m,\,x}$ is the transconductance of the transistor M_{x1} (and M_{x2}). The potential difference V_{xy} is generated from the voltage drop across a tunable resistor R such that $V_{xy} = I_b R$. With this setup, the effective transconductance of the main transconductor can be written as in the equation below:

$$g_{m,\,\mathrm{eff}} = \frac{k g_{m,\,x} I_b R}{2\eta V_{\mathrm{T}}} \tag{6}$$

$$= \frac{k I_b^2 R}{4(\eta V_{\mathrm{T}})^2} \tag{7}$$

The transconductor can be tuned by tuning the resistance R. The diode-connected transistors M_{x4} and M_{x5} set the common-mode bias for the differential pair.

3 Filter realisation

A filter with tunable bandwidth that extracts most biopotential signals is widely preferred to enhance the re-usability of the filter and for cost minimisation. This paper focuses on the design of such tunable low-pass filter which is capable of handling different biopotential signals such as electrocardiogram (ECG), electroencephalogram (EEG) and electromyography.

A fully differential filter realised using fully differential transconductors requires common-mode feedback (CMFB) circuit to set common-mode voltage levels of each integrating node equal (preferably to input common-mode level). An nth-order fully differential low-pass filter requires n CMFB circuits, demanding additional area, power and circuit complexity. We propose a method to realise a fully differential filter using the transconductor shown in Fig. 1, without the need for CMFB circuits. The method is explained with the help of a first-order filter.

3.1 First-order filter

A common architecture of a first-order fully differential low-pass $g_m - C$ filter is shown in Fig. 3, the transfer function of which is given by the equation below:

$$\frac{v_{op} - v_{om}}{v_{ip} - v_{im}} = \frac{1}{1 + (s/\omega_{\mathrm{o}})} \tag{8}$$

where $\omega_{\mathrm{o}} = (g_{m,\,\mathrm{eff}}/C)$ is the filter bandwidth.

The pseudo-differential version of the first-order filter shown in Fig. 3 has been realised using the proposed low-g_m cell shown in Fig. 1. The scheme of realisation is shown in Fig. 4*a* and is explained as follows.

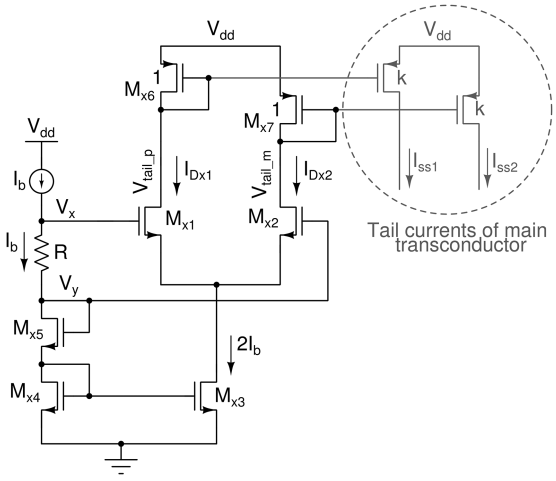

Fig. 2 *Tail currents generation circuit*

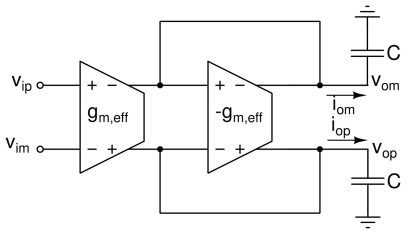

Fig. 3 *First-order fully differential $g_m - C$ filter*

The g_m cell along with an N-channel metal–oxide–semiconductor (MOS) current mirror load provides a single-ended output. Two such arrangements (leg-1 and leg-2 in the figure) together provide pseudo-differential output. For leg-1, the transconductor inputs v_{ip2} and v_{im2} are drawn from v_{om} and v_{op} of the differential output. From (1) and with the assumption $v_{\mathrm{i}p} = -v_{\mathrm{i}m}$ and $v_{\mathrm{o}p} = -v_{\mathrm{o}m}$, the output current $i_{\mathrm{o}p} = i_1 - i_2$ can be written as

$$i_{\mathrm{o}p} = i_1 - i_2 = g_{m,\,\mathrm{eff}}\left(v_{\mathrm{i}p} - v_{\mathrm{o}p}\right) \tag{9}$$

The resulting transfer function $(v_{\mathrm{o}p}/v_{\mathrm{i}p})$ takes the form given in (8). The leg-2 provides $i_{\mathrm{o}m}$ and $v_{\mathrm{o}m}$, and are derived by interchanging $v_{\mathrm{i}p}$ with $v_{\mathrm{i}m}$ and $v_{\mathrm{o}p}$ with $v_{\mathrm{o}m}$ at the input terminals of g_m-cell.

Note that, because of feedback, the output common-mode is set equal to the input, provided the DC gain is sufficiently large. However, the proposed arrangement is limited by the common-mode range requirement. This is due to the fact that the common-source nodes ($A1$ and $A2$ in leg-1; B_1 and B_2 in leg-2) experience a large signal swing for in-band frequencies, and therefore they are no longer at small-signal ground. For example, the swing at the node A_1 is influenced by $v_{\mathrm{i}p}$ and $v_{\mathrm{o}p}$, and both $v_{\mathrm{i}p}$ and $v_{\mathrm{o}p}$ are swinging almost equal for in-band frequencies. A careful look at the two legs reveals that nodes A_1 and B_1 (similarly, nodes A_2 and B_2) experience equal but opposite signal excursions. Joining these nodes will force the nodes to the small-signal ground, thus offering a fully differential version of the filter. This modification has been shown by dotted lines in Fig. 4*a*. This is not the case with the simple cross-coupled differential pair shown in Fig. 1. The common-source nodes here is not at small-signal ground (the two inputs are not differential) and there is going to be a signal-dependent common-mode voltage. Thus, the proposed architecture in Fig. 4 has a better linearity when compared with Fig. 1. The simplified schematic representation of the fully differential first-order block is shown in Fig. 4*b*.

The transistor sizes for the proposed filter with the biasing circuit, designed in 0.18 µm complementary MOS (CMOS) process from united microelectronics corporation (UMC) technologies, are listed in Table 1. The gate lengths (L) of the

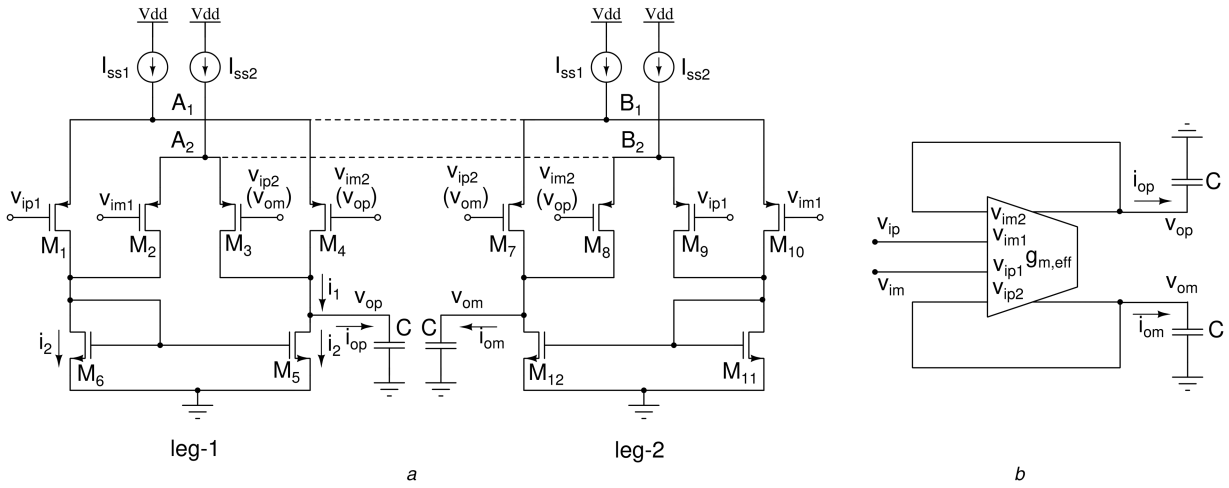

Fig. 4 *Scheme of realisation*

(a) Complete schematic representation of differential first-order $g_m - C$ filter, ***(b)*** Simplified schematic representation of the fully differential first-order block

Table 1 Transistor sizes of the proposed filter and biasing circuit

Transistor	$W(\mu\text{m})/L(\mu\text{m})$
M_{1-4}, M_{7-10}	2(0.25/48)
$M_{5,6}$, $M_{11,12}$	2(2/48)
$M_{x1,x2}$	2(1/48)
M_{x3-x5}	2(2/48)
$M_{x6,x7}$	2(2/48)
mirroring ratio $k = 1$	—

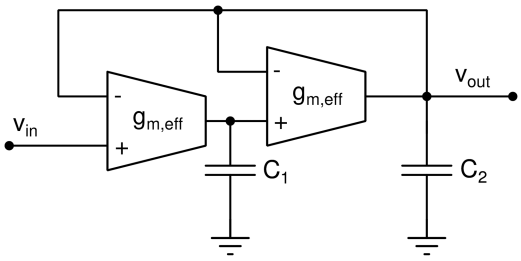

Fig. 5 *Single-ended second-order low-pass $g_m - C$ filter*

transistors are kept much higher than the width (W) for the following two reasons:

i. To maintain a sufficiently large output resistance of the filter so as to get a decent DC gain.
ii. To reduce g_m of each transistor, so that the effective transconductance ($g_{m1} - g_{m2}$) is made sufficiently small.

Usage of large L for all transistors also helps to increase the output resistance of transistors and thus to achieve accurate current mirroring. In addition, the resulting large gate area helps in minimising the effect of mismatch and the dominant flicker noise [8].

3.2 Fourth-order low-pass filter

A fourth-order low-pass Butterworth filter has been realised as a cascade of second-order sections. The second-order filter can be easily realised from the first-order filter shown in Fig. 4*b*, if one uses the architecture shown in Fig. 5 [9].

The transfer function of the second-order filter is given by

$$\frac{V_{\text{out}}(s)}{V_{\text{in}}(s)} = \frac{\omega_{\text{o}}^2}{s^2 + (\omega_{\text{o}}/Q)s + \omega_{\text{o}}^2} \tag{10}$$

where the pole frequency ω_{o} and the quality factor Q of the filter can be written as in (11) and (12), respectively

$$\omega_{\text{o}} = \frac{g_{m,\,\text{eff}}}{\sqrt{C_1 C_2}} \tag{11}$$

$$Q = \sqrt{\left(\frac{C_2}{C_1}\right)} \tag{12}$$

Schematic representation of the fully differential fourth-order Butterworth low-pass filter is shown in Fig. 6. The value of Q for each second-order section in the filter is taken from the filter table [10]. For a given $g_{m,\,\text{eff}} = 2\,\text{nS}$ and for Q values from the filter table, the integrating capacitances for each second-order section are computed using (11) and (12).

3.3 Switched transconductor filter

The bandwidth tuning scheme of tuning the resistor R, proposed in Section 2.1, is limited by the increase in flicker noise and reduction in DC gain on the lower frequencies. To reduce the cut-off frequency further, we use the filter based on switched/clocked transconductor in which the output current of the transconductor is switched to reduce the average output current, hence reducing the effective g_m [11]. The schematic representation of a fully differential second-order filter switched at the output of the transconductor is shown in Fig. 7. Here, a switch is included between the output of the filter and capacitor. The phase ϕ of the clock decides the duty ratio (D) of the switch, and in this phase the integrating capacitors integrate the currents. During the phase $\bar{\phi}$,

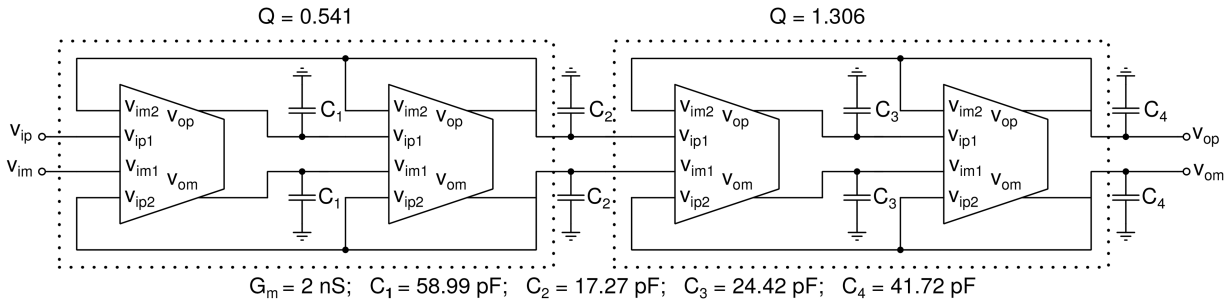

Fig. 6 *Fourth-order fully differential $g_m - C$ filter*

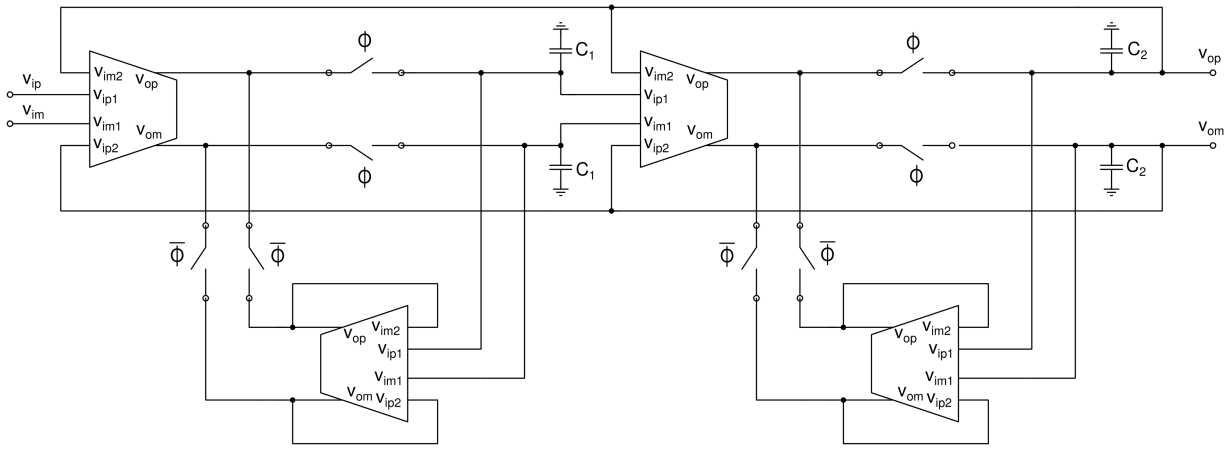

Fig. 7 *Second-order fully differential switched $g_m - C$ filter*

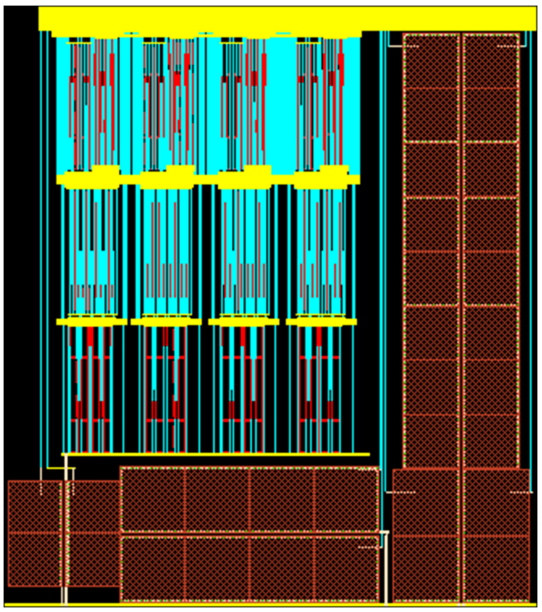

Fig. 8 *Layout of the proposed fourth-order fully differential low-pass filter with biasing circuit*

the transconductor currents are removed from capacitors and bypassed to transconductors dedicated for this purpose. This arrangement prevents the transconductor output from saturating. The effective transconductance of this arrangement is $Dg_{m,\,\mathrm{eff}}$. The switching also scales the output impedance and thus helps in maintaining DC gain at low (sub-hertz) bandwidth settings. The clock frequency must be chosen higher than the filter stop-band frequency. A fourth-order filter is realised by cascading two sections.

4 Simulation results

The g_m reduction scheme is validated through a fourth-order Butterworth low-pass filter designed in UMC 0.18 µm CMOS technology. Cadence Virtuoso 6.1.6 tool has been used for all designs and simulations. The filter is designed to have a tuning range from 1 to 70 Hz (for R variation) and 30 mHz to 100 Hz (for duty-ratio variation). All transistors are designed to operate in sub-threshold region. For the given transconductance of 2 nS and Bandwidth of 50 Hz, the intended capacitances for each second-order section are computed. For the 1st second-order section (with $Q = 0.541$), the value of capacitors is found to be $C_1 = 58.99$ pF and $C_2 = 17.272$ pF. Similarly, for the 2nd second-order section (with $Q = 1.306$), the values of capacitors are $C_3 = 24.424$ pF and $C_4 = 41.716$ pF.

Fig. 8 shows the layout for fully differential fourth-order filter shown in Fig. 6 (with only R-tuning). The total layout area is 0.91 mm × 0.81 mm. The magnitude response of the filter for R-tuning is shown in Fig. 9*a*. In Fig. 9*b*, bandwidth f_c as a function of the resistor R is plotted. It can be clearly seen that f_c is a linear function of R. An off-chip resistor (potentiometer) is preferred for R, over the on-chip resistor, as it is required to be tuned. Monte Carlo simulation has been carried out to observe the effect of transistor mismatch on the bandwidth. Fig. 9*c* shows the distribution of f_c for 100 samples when the R is set for $f_c = 50$ Hz. Mean of about 49.36 Hz and a standard deviation of about 1.9 Hz are observed.

Simulations are carried out for variations across process corners, supply voltage and temperature, for a bandwidth setting of 50 Hz. The magnitude response of the filter at various process corners is shown in Fig. 10*a*. It is observed that the change in bandwidth is <10% at a nominal supply voltage of 1.8 V and at room temperature 27°C. Fig. 10*b* shows the magnitude response for variation in temperature from 0 to 80°C at typical corner and nominal supply voltage, the change in bandwidth is <12%. For the ±10% variation in supply voltage from the nominal value at room temperature and at typical process corner, the change in bandwidth observed is <1% as shown in Fig. 10*c*. These deviations can be tuned back by readjusting R appropriately.

Simulations are carried out on the schematic representation of the switched-g_m filter. Fig. 11*a* shows the magnitude response. For a bandwidth set to 100 Hz (with $D = 100\%$), the duty cycle is varied from 0.01 to 50%. Note that the clock frequency is adjusted

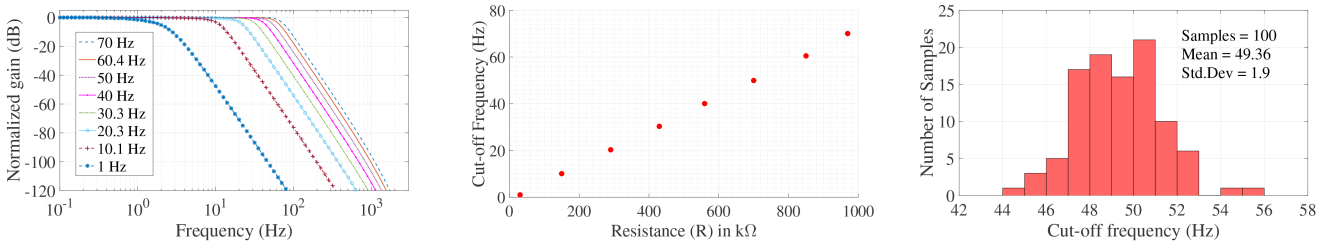

a *b* *c*

Fig. 9 *Magnitude response of the filter for R-tuning*

(a) Magnitude response of the filter with R tuning, ***(b)*** Tuning graph showing f_c for different values of R, ***(c)*** Monte Carlo simulation of the filter with 100 runs for $f_c = 50$ Hz setting

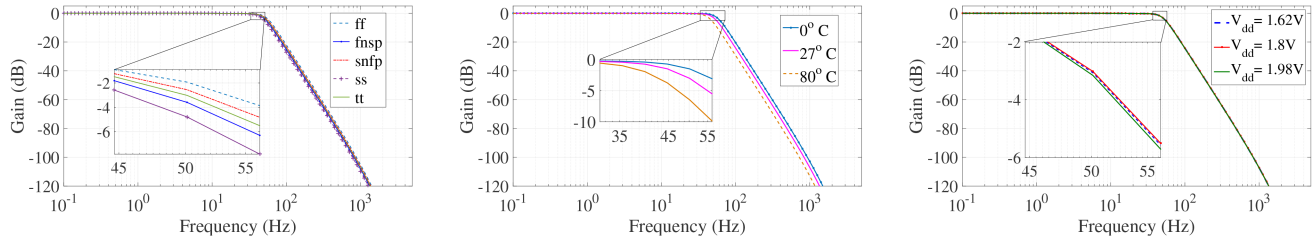

a *b* *c*

Fig. 10 *Magnitude response of the filter across*

(a) Process corner variations, ***(b)*** Temperature variations, ***(c)*** Supply variations

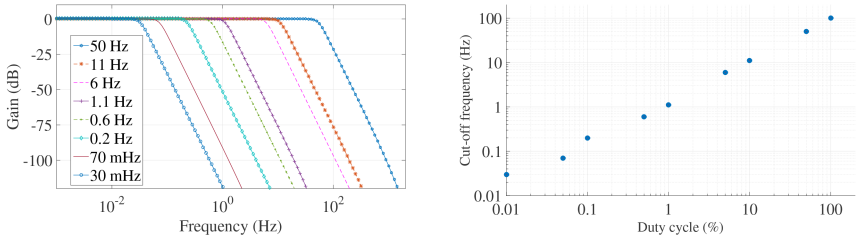

a *b*

Fig. 11 *Magnitude response*

(a) Magnitude response of the filter for duty-ratio tuning. The tuning range is from 50 Hz to 30 mHz. The settings used for these results are in the format [clock frequency, duty cycle, cut-off frequency]: [5 kHz, 50%, 50 Hz], [1 kHz, 10%, 11 Hz], [1 kHz, 5%, 6 Hz], [100 Hz, 1%, 1.1 Hz], [100 Hz, 0.5%, 0.6 Hz], [100 Hz, 0.1%, 0.2 Hz], [10 Hz, 0.05%, 70 mHz] and [10 Hz, 0.01%, 30 mHz], ***(b)*** Tuning graph showing the filter cut-off frequency for different duty cycles

Table 2 Summary of the filter performance at 1.8 V supply

Parameters	Filter-1	Filter-2
current consumption, μA	0.32	0.64
power, μW	0.57	1.14
DC gain, dB	0	0
filter order	4	4
bandwidth, Hz	1–70 Hz	30 mHz–100 Hz
linearity at 1% total harmonic distortion (THD)	196	188
($V_{\text{in},pk-pk}$ (mV) at 10 Hz)	—	—
input referred noise (IRN), μV_{rms}	109	129.2
(10 mHz–100 Hz)	—	—
dynamic range, dB	56.06	54.22

accordingly to keep clock feedthrough out of stop-band frequency (corresponding to the attenuation of 120 dB). The cut-off frequency is found to vary from 30 mHz to 50 Hz. Tuning graph showing f_c as a function of D is shown in Fig. 11*b*. The summary of the performances of two filters, Filter-1 (with only R-tuning) and Filter-2 (with fixed-R and tuned D) is shown in Table 2.

For biomedical signal processing, being the main application of the proposed filters, flicker noise is one of the important parameters of concern. Flicker noise of a transistor is inversely proportional to its W–L product (gate area) [12, 13]. It is to be noted that the gate area of the transistors in the proposed filter has been kept sufficiently large for the reasons outlined in Section 3.1, which in turn helps in keeping the flicker noise to a sufficiently low value.

The requirement on in-band input referred noise of the filter for a given input voltage and signal-to-noise ratio (SNR) is given by (as in [13])

$$\text{Noise}_{\text{in, ref}}(\text{rms}) \leq \frac{V_{\text{in, rms}}}{10^{\text{SNR(dB)}/20}} \tag{13}$$

In [13], it is also stated that for filtering biomedical signals such as ECG, the SNR requirement of the filter depends on maximum and minimum ECG levels and has been shown that the SNR requirement on the filter is ≥38 dB. Similarly, for EEG the requirement on SNR is 40 dB [14]. The proposed filters offer dynamic range in excess of 50 dB. This clearly shows that the noise contributed by proposed filters is well within the range to cause any significant performance degradation.

Note that Filter-1 and Filter-2 can process input voltage up to 196 mV_{pp} and 188 mV_{pp}, respectively. For SNR >40 dB, the input referred noise of these filters must be <692.96 and 664.68 μV_{rms}, respectively, as per (13). Therefore, the proposed filters offering input referred noise of 109 and 129.2 μV_{rms}, respectively, can definitely be good candidates for processing biomedical signals. Table 3 compares the simulation results of proposed filters to other low-frequency filters reported in the literature. For conciseness, only low-frequency filters with order four and above are included in this table. Both the proposed filters exhibit comparable dynamic range and figure-of-merit (FoM) when compared with recent papers in the literature.

Table 3 Comparison of the circuit performance with related works

Parameters	[15] (2007)	[13] (2009)	[16] (2012)	[17] (2013)	[18] (2016)	[19] (2017)	This work Filter-1	This work Filter-2
V_{DD}, V	1.8	1.5	3	±0.8	0.9	1	1.8	1.8
technology, μm	0.18	0.18	0.35	0.25	0.13	0.18	0.18	0.18
power, μW	200	0.453	0.75	30	2.8	0.35	0.57	1.14
DC gain, dB	–6	–9.5	–6	–5	5.9	–8	0	0
filter order	5	5	4	5	4	5	4	4
bandwidth, Hz	250	250	40	243	52	50	50	50
THD, dB	–44	–48.6	–59	–40	–40	–49.9	–40	–40
dynamic range, dB	52	50	54	65	43.22	49.8	56.06	54.22
IRN, μV_{rms}	266	340	500	36	24.4	97	109	129.2
FoM[a] ($\times 10^{-9}$)	100	0.286	0.374	3.3	4.83	0.226	0.224	0.554

[a]FoM [16] = $\frac{\text{power}}{\text{order} \times \text{dynamicrange}}$.

5 Conclusion

A novel technique is proposed for reducing g_m, for realising low-frequency $g_m - C$ filters. A technique to tune the effective transconductance is also presented. The proposed technique has been validated through simulations by designing a fourth-order low-pass Butterworth filter using transconductor cells. The architecture of g_m-cell makes it possible to realise a fully differential filter without the need for an explicit CMFB circuit. The simulation results justified that the proposed tuning scheme is linear. A tuning range of 1–70 Hz was achieved. The tuning range has been increased to 30 mHz–100 Hz by using a switched g_m-cell and modifying the filter circuit accordingly. Both the low-pass filters have exhibited comparable dynamic range and FoM with respect to state-of-the-art low-frequency filters. The proposed filter, because of its wide bandwidth tuning range, is a strong contender to be used in analogue front-end for processing biopotential signals.

6 Acknowledgment

The authors thank the Ministry of Electronics and Information Technology (MeitY), Government of India, for providing the EDA tools support through the SMDP-C2SD project.

7 References

[1] Harrison, R.R.: 'A versatile integrated circuit for the acquisition of biopotentials'. Proc. Custom Integrated Circuits Conf., San Jose, CA, USA, September 2007, pp. 115–122

[2] Nagaraj, K.: 'A parasitic-insensitive area-efficient approach to realizing very large time constants in switched-capacitor circuits', *IEEE Trans. Circuits Syst.*, 1989, **36**, (9), pp. 1210–1216

[3] Solis-Bustos, S., Silva-Martinez, J., Maloberti, F., *et al.*: 'A 60 dB dynamic-range CMOS sixth-order 2.4 Hz low-pass filter for medical applications', *IEEE Trans. Circuits Syst. II, Analog Digit. Signal Process.*, 2000, **47**, (12), pp. 1391–1398

[4] Veeravalli, A., Sanchez-Sinencio, E., Silva-Martinez, J.: 'Transconductance amplifier structures with very small transconductances: a comparative design approach', *IEEE J. Solid-State Circuits*, 2002, **37**, (6), pp. 770–775

[5] Zhou, L., Chakrabartty, S.: 'Design of low-G_m transconductors using varactor-based degeneration and linearization technique'. Proc. IEEE Biomedical Circuits and Systems Conf. (BioCAS), Atlanta, USA, October 2015, pp. 1–4

[6] Silva-Martinez, J., Salcedo-Suner, J.: 'IC voltage to current transducers with very small transconductance', *Analog Integr. Circuits Signal Process.*, 1997, **13**, (3), pp. 285–293

[7] Alioto, M.: 'Understanding DC behavior of subthreshold CMOS logic through closed-form analysis', *IEEE Trans. Circuits Syst. I, Regul. Pap.*, 2010, **57**, (7), pp. 1597–1607

[8] Akbari, M., Hashemipour, O., Moradi, F.: 'Input offset estimation of CMOS integrated circuits in weak inversion', *IEEE Trans. Very Large Scale Integr. (VLSI) Syst.*, 2018, **26**, (9), pp. 1812–1816

[9] Chang, C.M.: 'New multifunction OTA-C biquads', *IEEE Trans. Circuits Syst. II, Analog Digit. Signal Process.*, 1999, **46**, (6), pp. 820–824

[10] Schaumann, R., Valkenburg, M.E.V.: '*Design of analog filters*' (Oxford University press, USA, 2001)

[11] Rodriguez-Villegas, E., Casson, A.J., Corbishley, P.: 'A subhertz nanopower low-pass filter', *IEEE Trans. Circuits Syst. II, Express Briefs*, 2011, **58**, (6), pp. 351–355

[12] Veeravalli, A., Sanchez-Sinencio, E., Silva-Martinez, J.: 'A CMOS transconductance amplifier architecture with wide tuning range for very low frequency applications', *IEEE J. Solid-State Circuits*, 2002, **37**, (6), pp. 776–781

[13] Lee, S.Y., Cheng, C.J.: 'Systematic design and modeling of an OTA-C filter for portable ECG detection', *IEEE Trans. Biomed. Circuits Syst.*, 2009, **3**, (1), pp. 53–64

[14] Bronzino, J.D.: '*Medical devices and systems*' (CRC press, Boca Raton, Florida, USA., 2006, 3rd edn.)

[15] Lo, T.-Y., Hung, C.-C.: 'A wide tuning range G_m–C continuous-time analog filter', *IEEE Trans. Circuits Syst. I, Regul.Pap.*, 2007, **54**, (4), pp. 713–722

[16] Liu, Y.T., Lie, D.Y.C., Hu, W., *et al.*: 'An ultralow-power CMOS transconductor design with wide input linear range for biomedical applications'. Proc. IEEE Int. Symp. Circuits and Systems (ISCAS), Seoul, Korea (South), May 2012, pp. 2211–2214

[17] Mahmoud, S., Bamakhramah, A., Al-Tunaiji, S.: 'Low-noise low-pass filter for ECG portable detection systems with digitally programmable range', *Circuits Syst. Signal Process. J.*, 2013, **32**, (9), pp. 2029–2045

[18] Richa, A., Oliveira, J.P.: 'G_m–C biquad filter for low signal sensor applications'. Proc. MIXDES-23rd Int. Conf. Mixed Design of Integrated Circuits and Systems, Poland, 2016, pp. 207–210

[19] Sun, C.-Y., Lee, S.-Y.: 'A fifth-order Butterworth OTA-C LPF with multiple-output differential-input OTA for ECG applications', *IEEE Trans. Circuits Syst. II, Express Briefs*, 2017, **65**, (4), pp. 421–425